High-Pressure Study of Oxo-bridged Mixed-Valent Mn-III/Mn-IV Dimers

High-Pressure Study of Oxo-bridged Mixed-Valent Mn^{III}/Mn^{IV} Dimers

Alessandro Prescimone[a], Javier Sanchez-Benitez[b], Konstantin V. Kamenev[b], John E. Warren[c], Alistair R. Lennie[c], Mark Murrie[d], Simon Parsons[a], and Euan K. Brechin[a]

[a] School of Chemistry and Centre for Science at Extreme Conditions, The University of Edinburgh, West Mains Road, Edinburgh, EH9 3JJ, UK
[b] School of Engineering and Centre for Science at Extreme Conditions, The University of Edinburgh, Mayfield Road, Edinburgh, EH9 3JZ, UK
[c] Synchrotron Radiation Source, STFC Daresbury Laboratory, Warrington, Cheshire, WA4 4AD, UK
[d] Department of Chemistry, University of Glasgow, University Avenue, Glasgow, G12 8QQ, UK

Reprint requests to Dr. Euan K. Brechin. Fax : +44-131-650-6453.
E-mail: ebrechin@staffmail.ed.ac.uk or s.parsons@ed.ac.uk

Z. Naturforsch. **2010**, *65b,* 221 – 230; received November 27, 2009

Dedicated to Professor Rolf W. Saalfrank on the occasion of his 70th birthday

A combination of high-pressure single crystal X-ray diffraction and high-pressure SQUID magnetometry has been used to study two oxo-bridged mixed-valent Mn^{III}/Mn^{IV} dimers. $[Mn_2O_2(bpy)_4](ClO_4)_3{\cdot}3CH_3CN$, (**1**$\cdot 3CH_3CN$; bpy = 2,2′-bipyridine) has been compressed to 2.0 GPa whilst $[Mn_2O_2(bpy)_4](PF_6)_3{\cdot}2CH_3CN{\cdot}1H_2O$, (**2**$\cdot 2CH_3CN{\cdot}1H_2O$) could be measured crystallographically up to 4.55 GPa. The PF_6 salt of $[Mn_2O_2(bpy)_4]^{3+}$ has never been reported before while **1** has been reported as a hydrate and in a different crystallographic space group. The application of hydrostatic pressure imposes significant distortions and modifications in the structures of both complexes. In particular, in complex **1**$\cdot 3CH_3CN$ the Mn–Mn separation is reduced by the contraction of some of the Mn–O bond lengths, whilst in **2**$\cdot 2CH_3CN{\cdot}1H_2O$ the Mn–O–Mn bridging angles and the Mn–O bond lengths are substantially unchanged. Interestingly **2**$\cdot 2CH_3CN{\cdot}1H_2O$ also shows a constant contraction in nearly all the Mn–N bonds. The magnetic behaviour of the complexes has been measured up to 0.87 GPa for **1**$\cdot 3CH_3CN$ and 0.84 GPa for **2**$\cdot 2CH_3CN{\cdot}1H_2O$.

Key words: High Pressure, Coordination Chemistry, Clusters, X-Ray Crystallography, SQUID Magnetometry

Introduction

In the early 1950s [1], in a study that began with copper acetate, it was discovered that it was possible to determine a theoretical expression that relates the magnetic susceptibility as function of temperature to various structural parameters. Perhaps one of the most influential breakthroughs in the field was the discovery in the 1970s [2] of the relationship between the coupling constant (J) and the Cu–O–Cu bridging angle (α) in hydroxo-bridged Cu^{II} dimers. This was an important result because it facilitated estimation of the nature and magnitude of the magnetic interactions between metal centres in new complexes simply from initial crystallographic observations. In particular an antiferromagnetic interaction is to be expected if $\alpha > 97.5°$, and a ferromagnetic interaction is to be expected if $\alpha < 97.5°$. Since this discovery, much work has been done to improve and enhance this result, and to achieve similar magneto-structural correlations for different families of dinuclear systems containing first row transition metals [3 – 10]. Such studies require the synthesis of several analogous compounds, and this can lead to some practical difficulties because it may not be simple to prepare a large library of molecules with the same magnetic core. To achieve this, different organic co-ligands, solvents and/or counter ions must be employed, and their role assumed to be purely innocent, *i. e.* bar changes in geometry, they have no *direct* influence on the magnetism.

The ideal solution would be to twist, bend and stretch *exactly* the same molecule. Chemically this is essentially impossible, but with advances in technology a suitable alternative that is becoming more

Table 1. Crystal structure data for **1**·3CH_3CN as function of pressure.

Pressure, GPa	ambient	0.18	1.00	2.00
T, K	150	300	300	300
M_r	1188.11	1188.11	1188.11	1188.11
Crystal size, mm^3	$0.23 \times 0.18 \times 0.11$	$0.14 \times 0.12 \times 0.08$	$0.14 \times 0.12 \times 0.08$	$0.14 \times 0.12 \times 0.08$
Crystal system	triclinic	triclinic	triclinic	triclinic
Space group	$P\bar{1}$	$P\bar{1}$	$P\bar{1}$	$P\bar{1}$
a, Å	13.2108(2),	13.2520(8)	12.969(3),	12.657(4)
b, Å	13.7331(3)	13.8270(8)	13.5755(14)	13.394(2)
c, Å	16.0434(3)	16.0093(11)	15.7245(14)	15.538(3)
α, deg	65.4150(10)	65.446(5)	64.279(5)	63.47(1)
β, deg	72.0270(10)	71.915(6)	72.026(7)	71.93(1)
γ, deg	83.1960(10)	83.172(4)	83.282(8)	83.66(2)
V, $Å^3$	2517.49(9)	2536.2(3)	2372.0(6)	2239.1(11)
Z	2	2	2	2
D_{calcd}, g cm^{-3}	1.57	1.56	1.66	1.76
Wavelength; λ, Å	MoK_α; 0.71073	synchrotron; 0.48650	synchrotron; 0.48650	synchrotron; 0.48650
μ, mm^{-1}	0.7	0.2	0.2	0.3
$F(000)$, e	1214	1214	1214	1214
hkl range	$-18 \le h \le +18$ $-19 \le k \le +19$ $-22 \le l \le +22$	$-15 \le h \le +15$ $-16 \le k \le +16$ $-20 \le l \le +20$	$-13 \le h \le +13$ $-14 \le k \le +14$ $-16 \le l \le +16$	$-13 \le h \le +13$ $-14 \le k \le +14$ $-17 \le l \le +17$
θ_{max}, deg	30.0	17.7	15.7	15.7
Refl. measured	76562	15556	11178	10855
Refl. unique	14287	4212	2959	2769
R_{int}	0.037	0.093	0.071	0.110
Param. refined	712	225	225	225
$R\,[F \ge 2\sigma(F)]/wR(F)$	0.050 / 0.052	0.093 / 0.069	0.085 / 0.049	0.098 / 0.068
GoF (F)	1.16	1.01	1.00	0.99
$\Delta\rho_{fin}$ (max / min), e $Å^{-3}$	1.09 / −1.08	0.59 / −0.38	0.56 / −0.49	0.52 / −0.44

widely available is the application of "external" hydrostatic pressure. Science at extreme conditions has developed greatly in recent years affording suitable techniques [11], software [12 – 14], tools [15 – 18], and instrumentation [12, 19] both crystallographically and magnetically, that allow us to initiate these very studies. In particular high-pressure crystallographic techniques are already rather well established [20 – 27]. Reports employing high-pressure magnetic techniques on molecular systems are somewhat less common [28 – 32].

Despite the availability of these exciting new tools, there are, to the best of our knowledge, only a handful of studies that combine high-pressure single crystal X-ray diffraction and high-pressure SQUID magnetometry [33 – 37]. These reports demonstrate that by the application of pressure it is possible to distort intramolecular bond lengths and angles significantly, and that these structural changes are manifested in a concomitant change in the magnetic behaviour. In this paper we focus our high-pressure study on two mixed-valent oxo-bridged Mn^{III}/Mn^{IV} dimers, a family of compounds that has attracted interest from both a magnetic and biological viewpoint [38].

Results and Discussion

Description of structures

$[Mn_2O_2(bpy)_4](ClO_4)_3$·3$CH_3CN$, (**1**·3$CH_3CN$; bpy = 2,2′-bipyridine) has been previously reported as a hydrate in the monoclinic space group $P2_1/c$ [39]. The structures of **1**·3CH_3CN and $[Mn_2O_2(bpy)_4]$-$(PF_6)_3$·2CH_3CN·1H_2O, (**2**·2CH_3CN·1H_2O) are ana-

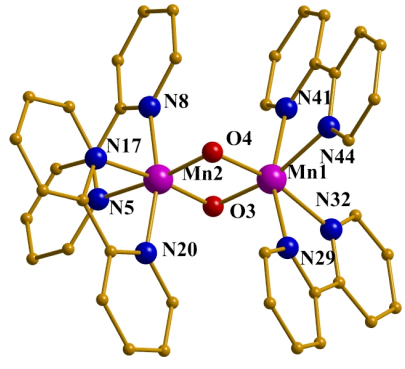

Fig. 1. The molecular structure of the complex cation in **1**·3CH_3CN and **2**·2CH_3CN·1H_2O. Colour scheme: Mn = violet, C = gold, O = red, N = blue. Counter ions, H atoms and solvent molecules omitted for clarity.

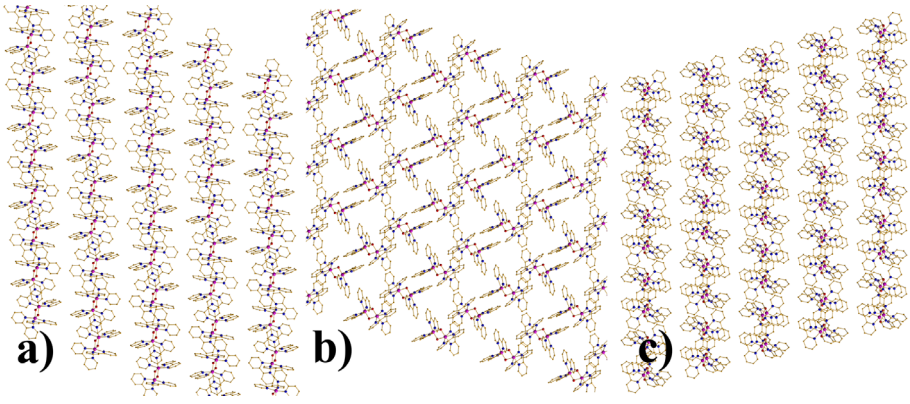

Fig. 2. Packing diagrams of **1**·3CH_3CN along the three crystallographic axes *a*, *b* and *c*.

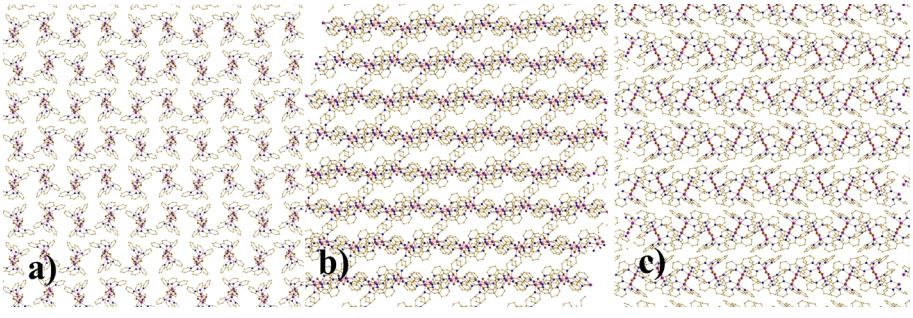

Fig. 3. Packing diagrams of **2** · 2 CH_3CN · 1 H_2O along the three crystallographic axes *a*, *b* and *c*.

logous (Fig. 1), containing a central mixed-valent $[Mn^{III}Mn^{IV}O_2]$ asymmetric rhomb of two Mn ions bridged by two μ-O^{2-} ligands. Two bpy ligands fulfil the octahedral coordination around each Mn atom, with charge balance maintained by the presence of three $[ClO_4]^-$ ions (**1**·3CH_3CN), or three $[PF_6]^-$ ions (**2**·2CH_3CN·1H_2O). Bond length considerations (see Tables 4 and 5) and BVS calculations reveal Mn1 to be 3+ and Mn2 to be 4+. In each case the Jahn-Teller axis of the Mn^{3+} ion is defined by the N–Mn–N vector which is approximately perpendicular to the $[Mn_2O_2]$ plane. The Mn–Mn separation and the O–Mn–O bridging angles are 2.7058(4) Å, 96.42(7)°, and 96.09(7)° in **1**·3CH_3CN and 2.7177(7) Å, 97.00(11)°, and 96.97(11)° in **2**·2CH_3CN·1H_2O.

There are three CH_3CN molecules of solvation per dimer in the crystal of **1**·3CH_3CN, two CH_3CN and one H_2O molecule in the crystal of **2**·2CH_3CN·1H_2O. In each case the solvent molecules and anions are hydrogen-bonded to the protons of the bpy rings at distances of approximately 2.6 Å, with the closest inter-cluster interactions being between staggered π-π-stacked bpy rings at approximately 3.6 Å (C···C). Packing diagrams illustrating the views along the three crystallographic axes are shown in Figs. 2 and 3.

Refinement of the high-pressure crystal structures

Although it was possible to refine the data of compound **1**·3CH_3CN with all three solvent molecules at every pressure, the same could not be achieved for **2**·2CH_3CN·1H_2O, and the SQUEEZE [40] routine was used to treat one CH_3CN molecule and the water molecule at ambient pressure and all the solvent at high pressure. The input to the SQUEEZE procedure consists of the ordered part of the structure; voids in the ordered model are located, and an electron density synthesis calculated in these void regions. The electron density found is back transformed into 'solvent' contributions to the structure factors. The results of the SQUEEZE calculations are reported in Table 3, which lists the volume of the solvent region and the number of electrons (per cell) treated by the procedure.

The solvent in the crystal structure of **2**·2CH_3CN ·1H_2O was badly disordered (even at high pressure), and little progress could be made during refinement using partial-occupancy atomic models. However, the SQUEEZE routine is based on a Fourier transformation, and this will be distorted if a data set is not complete. For this reason the SQUEEZE routine can be unstable when used with high-pressure data, since the pressure

Table 2. Crystal structure data for **2**·$2CH_3CN$·$1H_2O$ as function of pressure.

Pressure, GPa	ambient	0.45	1.23	1.75	3.00	4.55
T, K	150	300	300	300	300	300
M_r	1301.61	1301.61	1301.61	1301.61	1301.61	1301.61
Crystal size, mm^3	0.22×0.18×0.12	0.14×0.13×0.09	0.14×0.13×0.09	0.14×0.13×0.09	0.14×0.13×0.09	0.14×0.13×0.09
Crystal system	monoclinic	monoclinic	monoclinic	monoclinic	monoclinic	monoclinic
Space group	$P2_1/n$	$P2_1/n$	$P2_1/n$	$P2_1/n$	$P2_1/n$	$P2_1/n$
a, Å	13.3430(3)	13.3300(4)	12.9086(5)	12.7539(5)	12.4580(6)	12.2052(6)
b, Å	21.7678(5)	21.7458(11)	21.5215(15)	21.4355(14)	21.2622(19)	21.0264(18)
c, Å	18.2512(4)	18.0899(9)	17.5207(13)	17.3277(11)	16.9537(16)	16.6200(16)
β, deg	103.6750(10)	103.272(3)	101.683(4)	101.105(4)	100.128(5)	99.439(5)
V, $Å^3$	5150.7(2)	5103.7(4)	4766.6(5)	4648.5(5)	4420.8(6)	4207.5(6)
Z	4	4	4	4	4	4
D_{calcd}, g cm^{-3}	1.68	1.68	1.80	1.84	1.94	2.04
Wavelength; λ, Å	MoK_α; 0.71073	synchrotron; 0.48630	synchrotron; 0.48630	synchrotron; 0.48630	synchrotron; 0.48630	synchrotron; 0.48630
μ, mm^{-1}	0.7	0.2	0.2	0.2	0.2	0.3
F(000), e	2992	2992	2992	2992	2992	2992
hkl range	$-17 \le h \le +17$ $0 \le k \le +29$ $0 \le l \le +23$	$-14 \le h \le +14$ $-21 \le k \le +22$ $-17 \le l \le +17$	$-14 \le h \le +14$ $-21 \le k \le +22$ $-17 \le l \le +17$	$-14 \le h \le +14$ $-20 \le k \le +22$ $-17 \le l \le +17$	$-13 \le h \le +13$ $-21 \le k \le +22$ $-17 \le l \le +16$	$-13 \le h \le +13$ $-21 \le k \le +21$ $-17 \le l \le +16$
θ_{max}, deg	28.9	15.7	15.9	15.7	15.7	15.8
Refl. measured	62474	18044	17122	15620	14835	13529
Refl. unique	12766	4187	3963	3633	3454	3205
R_{int}	0.061	0.100	0.101	0.092	0.125	0.120
Param. refined	670	658	658	658	658	658
$R\,[F \ge 2\sigma(F)]/wR(F)$	0.051 / 0.060	0.076 / 0.065	0.067 / 0.055	0.061 / 0.046	0.078 / 0.080	0.079, 0.078
GoF (F)	0.93	0.99	1.00	1.00	1.02	1.10
$\Delta\rho_{fin}$ (max / min), e $Å^{-3}$	1.14 / −0.77	0.47 / −0.32	0.47 / −0.35	0.49 / −0.35	0.68 / −0.68	0.65, −0.62

cell body results in shading of the diffraction pattern, leading to data sets of low completeness. The data in Table 3 illustrate some of the disadvantages of using the SQUEEZE routine with high-pressure data. The volume of the solvent void treated in the ambient-pressure refinement was larger than in the high-pressure refinements because one MeCN molecule was modelled explicitly. Nevertheless the electron count is similar at ambient pressure and 0.45 GPa whereas it should be bigger to account for the extra MeCN molecules per cell now being treated using SQUEEZE. Rather than indicating that some solvent is being pushed out of the crystal as pressure increases, the most likely explanation for this is that the electron density integration is biased by the low completeness (*ca.* 53 % on average) of the high-pressure data collections. This being said, the high-pressure data sets all have similar completeness, with the same region of reciprocal space being sampled for every pressure. It seems reasonable to assume that what ever the bias is in the SQUEEZE integration it should be consistent across each data set. If this assumption is correct the abrupt increase in the electron count at 3.00 GPa does appear to indicate that some surrounding hydrostatic medium is being pushed into the crystal voids. A similar effect has been observed in the porous zeolitic imidazole framework ZIF-8 at high pressure [41].

Table 3. SQUEEZE results for **2**·$2CH_3CN$·$1H_2O$ as function of pressure.

Pressure, GPa	Vol ($Å^3$)	N° e^- per cell	Asymmetric unit modeled after SQUEEZE applied
Ambient	504	125	**2**·$1CH_3CN$
0.45	844	130	**2**
1.23	701	136	**2**
1.75	648	126	**2**
3.00	564	164	**2**
4.55	476	162	**2**

Effect of pressure on structures

The unit cells of both compounds contract as pressure increases (Tables 1 and 2). It should be noted that compound **1**·$3CH_3CN$ has a slightly larger cell volume at 0.18 GPa and 300 K (2517.49(9) $Å^3$) than at ambient pressure and 150 K (2536.2(3) $Å^3$); in this case 0.18 GPa of pressure is not enough to overcome thermal expansion. Two perchlorate anions which are disordered in the low-temperature, ambient-pressure structure become ordered at 0.18 GPa. Perchlorate an-

Pressure, GPa	Ambient	0.18	1.00	2.00
Mn1–O3	1.8419(15)	1.823(7)	1.834(8)	1.817(11)
Mn1–O4	1.8621(15)	1.842(13)	1.908(15)	1.78(2)
Mn1–N44	2.1093(19)	2.084(5)	2.082(6)	2.072(8)
Mn1–N41	2.2053(18)	2.219(4)	2.226(4)	2.194(7)
Mn1–N32	2.1666(19)	2.173(12)	2.232(12)	2.245(16)
Mn1–N29	2.2221(18)	2.163(4)	2.162(4)	2.142(6)
Mn2–O3	1.7867(15)	1.749(14)	1.781(15)	1.79(2)
Mn2–O4	1.7753(15)	1.778(7)	1.756(8)	1.740(10)
Mn2–N5	2.0971(18)	2.078(5)	2.123(6)	2.144(8)
Mn2–N8	2.0160(18)	2.008(4)	2.014(4)	2.002(6)
Mn2–N17	2.0813(18)	2.074(10)	2.065(9)	2.060(13)
Mn2–N20	2.0165(18)	1.996(4)	2.007(4)	2.021(5)
Mn1–Mn2	2.7058(4)	2.700(2)	2.688(2)	2.676(4)
Mn1–O3–Mn2	96.42(7)	98.1(7)	96.1(7)	95.6(11)
Mn1–O4–Mn2	96.09(7)	96.6(7)	94.3(7)	98.7(11)

Table 4. Selected bond lengths (Å) and angles (deg) for **1**·3CH_3CN as function of pressure (estimated standard deviations in parentheses).

Table 5. Selected bond lengths (Å) and angles (deg) for **2**·2CH_3CN·1H_2O as function of pressure (estimated standard deviations in parentheses).

Pressure, GPa	Ambient	0.45	1.23	1.75	3.00	4.55
Mn1–O3	1.847(2)	1.833(7)	1.835(7)	1.833(6)	1.824(9)	1.828(10)
Mn1–O4	1.850(2)	1.831(6)	1.839(7)	1.835(6)	1.839(9)	1.821(11)
Mn1–N44	2.134(3)	2.144(7)	2.127(7)	2.127(6)	2.097(8)	2.084(9)
Mn1–N41	2.220(3)	2.207(6)	2.193(6)	2.178(5)	2.178(7)	2.156(8)
Mn1–N32	2.128(3)	2.137(6)	2.115(6)	2.113(6)	2.086(8)	2.085(9)
Mn1–N29	2.212(3)	2.189(5)	2.178(5)	2.173(5)	2.157(7)	2.148(8)
Mn2–O3	1.781(2)	1.773(6)	1.786(6)	1.792(6)	1.767(9)	1.752(12)
Mn2–O4	1.779(2)	1.781(7)	1.795(7)	1.797(6)	1.797(9)	1.791(11)
Mn2–N5	2.077(3)	2.072(6)	2.077(6)	2.067(6)	2.054(8)	2.029(8)
Mn2–N8	2.008(3)	2.002(5)	2.002(5)	2.004(5)	1.992(7)	1.998(8)
Mn2–N17	2.078(3)	2.090(6)	2.064(6)	2.058(6)	2.035(8)	2.017(9)
Mn2–N20	2.017(3)	2.023(6)	2.009(6)	2.013(5)	2.003(7)	1.982(8)
Mn1–Mn2	2.7177(7)	2.706(2)	2.702(2)	2.698(2)	2.691(3)	2.672(3)
Mn1–O3–Mn2	97.00(11)	97.1(3)	96.5(4)	96.3(3)	97.0(5)	96.5(4)
Mn1–O4–Mn2	96.97(11)	97.1(3)	96.1(3)	96.0(3)	95.5(5)	95.4(5)

ions are notoriously susceptible to disorder even at low temperature, as seen here for **1**·3CH_3CN at 150 K, and it is notable that in this case high pressure was a more effective means to force the structure to become ordered, even at ambient temperature.

Intermolecular interactions are generally weak, and the compression in the crystal of **1**·3CH_3CN is mainly driven by the reduction of the voids (Figs. 4 and 5). Void volumes can be estimated using a tool available in PLATON [42], and at 0.18 GPa the void/volume ratio is approximately 4.5 % of the total unit cell volume, whereas at 2.00 GPa the ratio has decreased to 3 % (a probe radius of 0.8 Å was used for these calculations). The same observation cannot be made for compound **2**·2CH_3CN·1H_2O because of the uncertainty related to the presence or absence of solvent molecules.

Distortions of the intramolecular bond lengths and angles in **1**·3CH_3CN are also observed (Table 4). The Mn–Mn distance contracts from 2.7058(4) Å at ambient pressure to 2.676(4) Å at 2 GPa, likely due to the significant contraction of both Mn–O4 bonds. Alterations to the Mn–O3 distances are statistically insignificant and so is the behaviour of the Mn1–O4–Mn2 angle. There are also significant changes in the Mn1(Mn^{3+})–N bond lengths, which see two of the four decreasing and one (N32) increasing (Table 4). The Jahn-Teller axis (N41–Mn1–N29), is significantly shortened as the Mn1–N29 bond contracts from 2.2221(18) Å down to 2.142(6) Å. For Mn2 (Mn^{4+}) the changes are less significant, with the exception of the Mn1–N5 bond which increases from 2.078(5) at 0.18 GPa to 2.144(8) Å at 2.00 GPa.

2·2CH_3CN·1H_2O shows essentially analogous behaviour: the Mn–Mn distance is contracted from 2.7177(7) Å at ambient pressure to 2.672(3) Å at 4.55 GPa. It seems likely that this change should be accompanied by a decrease in the Mn–O distances and Mn–O–Mn angles, but, because the standard un-

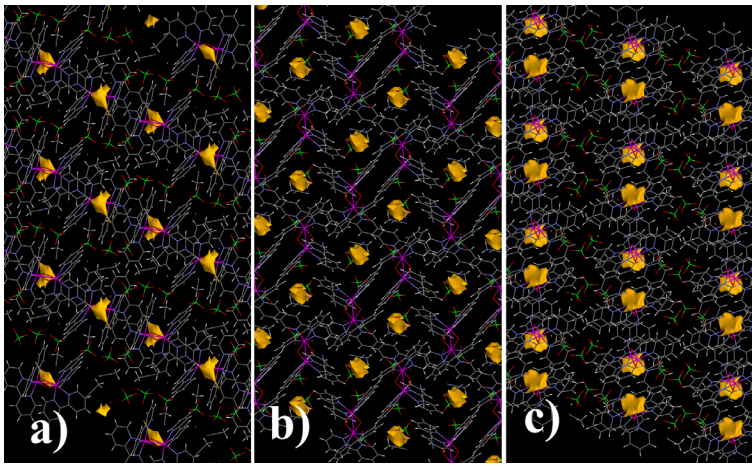

Fig. 4. Void diagrams of **1**·3CH_3CN along the three crystallographic axes *a*, *b* and *c* at 0.18 GPa. Probe size: 0.8 Å.

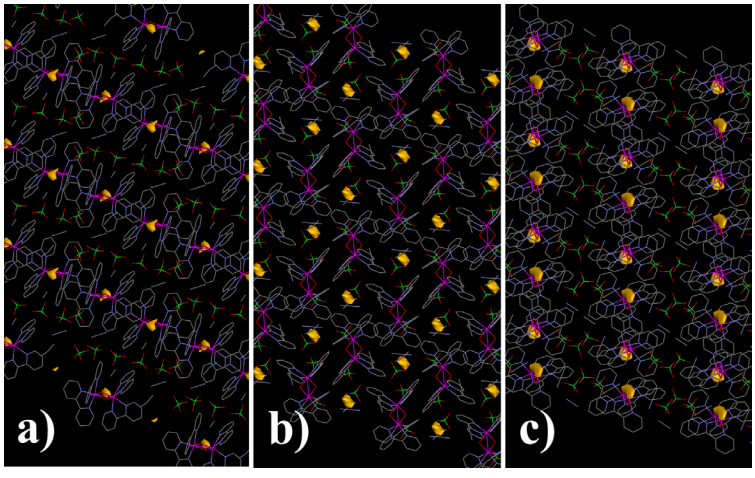

Fig. 5. Void diagrams of **1**·3CH_3CN along the three crystallographic axes *a*, *b* and *c* at 2.00 GPa. Probe size: 0.8 Å.

certainties at high pressure are large, the variations observed (Table 5) are not statistically significant. For Mn1(Mn^{3+}) all four bonds to the N atoms shrink significantly (Table 5), and the same trend is observed in three of the four Mn2(Mn^{4+})–N bonds. These bond length changes are somewhat unusual as all our previous studies on transition metal cluster complexes have shown them to be somewhat resistant to pressure effects [36, 37]. Our attempts to analyse the structures at higher pressures were unfortunately hindered by the degradation of the crystals.

Effect of pressure on magnetism

Variable-temperature magnetic susceptibility data were collected on **1**·3CH_3CN and **2**·2CH_3CN·1H_2O in the temperature range 350 – 20 K in an applied field of 1 kG at ambient and three different pressures and are plotted as the $\chi_m T$ product *versus* T in Figs. 6 and 7. The magnetic behaviour of **1**·3CH_3CN and **2**·2CH_3CN·1H_2O under ambient pressure is analogous to that previously reported for the monoclinic analogue of **1**·3CH_3CN [43]. Simulations of the susceptibility data (Figs. 4 and 5) using the Hamiltonian of Eq. 1 suggest strong antiferromagnetic exchange in **1**·3CH_3CN ($J = -177$ cm^{-1}, $g = 1.96$) and in **2** ($J = -185$ cm^{-1}, $g = 1.98$) [44].

$$\hat{H} = -2J(\hat{S}_1 \cdot \hat{S}_2) \quad (1)$$

At all pressures and low temperatures ($T < 100$ K) the value of $\chi_m T$ for both complexes is constant at ~0.36 $cm^3\,K\,mol^{-1}$. Above 100 K the value then increases steadily with temperature reaching values of 0.66 $cm^3\,K\,mol^{-1}$ (**1**·3CH_3CN) and 0.64 $cm^3\,K\,mol^{-1}$ (**2**·2CH_3CN·1H_2O) at 350 K. As can be seen from Figs. 6 and 7 the variable pressure data sets are essentially super-imposable on

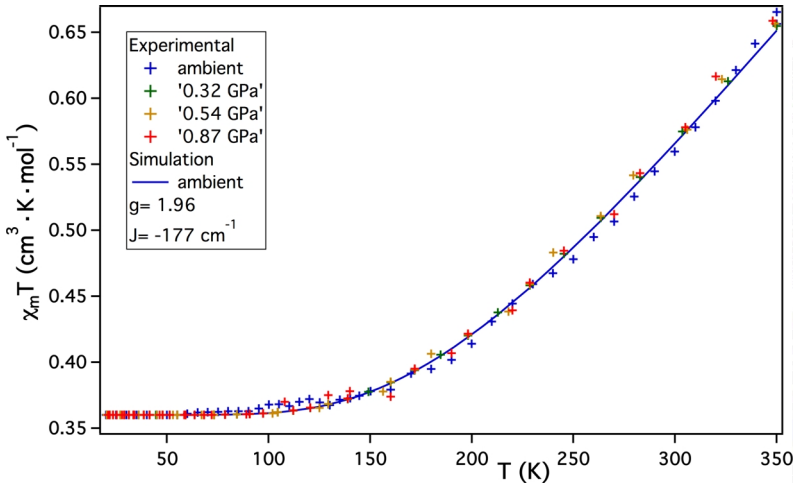

Fig. 6. Plots of $\chi_m T$ *versus* T for **1**·3CH_3CN recorded in the 350 – 20 K temperature range at the indicated pressures; the solid lines represent simulations of the data.

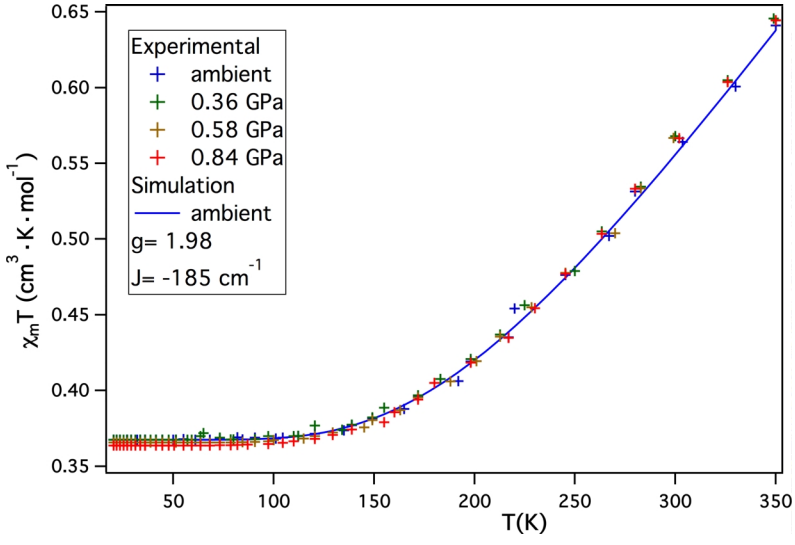

Fig. 7. Plots of $\chi_m T$ *versus* T for **2**·2CH_3CN·1H_2O recorded in the 350 – 20 K temperature range at the indicated pressures; the solid lines represent simulations of the data.

the ambient pressure data. The independence of the magnetic properties from pressure (up to 0.87 GPa for **1**·3CH_3CN and 0.84 GPa for **2**·2CH_3CN·1H_2O) is consistent with the minimal structural change below 1 GPa. Unfortunately, a lack of technology does not allow us to measure the susceptibility at the higher pressures where the major structural changes occurr [33, 34, 36, 37]. This work will require the design of new pressure cells which is on-going.

Conclusion

We have presented a rare example of the combined use of high-pressure magnetometry and high-pressure single-crystal X-ray crystallography to study two dinuclear oxo-bridged mixed-valent Mn^{III}/Mn^{IV} complexes. Magnetic data were recorded up to 0.87 GPa for **1**·3CH_3CN and 0.84 GPa for **2**·2CH_3CN·1H_2O, with structural data available up to 2.00 GPa for **1**·3CH_3CN and 4.55 GPa for **2**·2CH_3CN·1H_2O. The significant decrease in the cell volumes below 1 GPa occur *via* the compression of interstitial voids, with little change in the intra-molecular bond lengths and angles, and consequently there are no changes in the variable temperature susceptibility. Above 1 GPa the metal-metal separations decrease, and there are changes in both the bond lengths and bond angles that, in average, tend to decrease. The development of a new low-background pressure cell suitable for magnetic measurements above 1.0 GPa is in progress to investigate the magnetic behaviour of these

samples in the pressure range where structural modifications occur.

Experimental Section

All reactions were carried out in aerobic conditions using materials as received with no further purifications. $[Mn_2O_2(bpy)_4][ClO_4]_3\cdot 3CH_3CN$ (**1**·3CH_3CN) and $[Mn_2O_2(bpy)_4][PF_6]_3\cdot 2CH_3CN\cdot H_2O$ (**2**·2CH_3CN·1H_2O) were made as previously described [45].

General method

A solution of 4.3 g $Mn(OAc)_2\cdot 4H_2O$ (OAc = CH_3COO) (17.5 mmol) in 60 mL of H_2O was added to 8.2 g of 2,2′-bipyridine (52.5 mmol) in 30 mL of acetone with stirring. 80 mL of 1 M acetate buffer (pH = 5) was then added to the yellow solution, followed by 1.18 g of $KMnO_4$ (7.5 mmol) in 50 mL of H_2O. The resulting green solution was stirred for 15 min before $NaClO_4$ (4.5 g, 36.8 mmol) for **1**·3CH_3CN, or NH_4PF_6 for **2** (6.0 g, 36.5 mmol), was added to precipitate the product as a green powder. The product was first washed with ethanol and diethyl ether, and then recrystallised from acetonitrile to give brown-green crystals. – Anal. for **1**·3CH_3CN, $C_{46}H_{41}Cl_3Mn_2N_{11}O_{14}$: calcd. C 46.50, H 3.48, N 12.97; found C 46.23, H 3.28, N 12.84. – Anal. for **2**, $C_{44}H_{40}F_{12}Mn_2N_{10}O_3P_3$: calcd. C 44.50, H 3.39, N 11.79; found C 44.12, H 3.26, N 11.88.

X-Ray structure determination

High-pressure single-crystal experiments were carried out using a Merrill-Bassett diamond anvil cell (half-opening angle 40°) [46], equipped with Boehler-Almax diamonds with 600 μm culets and a tungsten gasket [16]. Petroleum ether was used as hydrostatic medium for all the compounds. A small ruby chip was loaded into the cell as the pressure calibrant with the ruby fluorescence used to measure the pressure [47]. Diffraction data were collected using synchrotron radiation of wavelength λ = 0.4865 Å for **1**·3CH_3CN and 0.4863 Å for **2**·2CH_3CN·1H_2O at r. t. on a Bruker Smart APEX II [12] diffractometer on Station 9.8 at SRS, Daresbury Laboratory [19]. Data collection and processing followed the procedures established by Dawson *et al.* [13]. Integrations were carried out using the program SAINT [48] and absorption corrections with the programs SADABS [49] and SHADE [14]. A key step in improving the data fitting in the structures of **2**·2CH_3CN·1H_2O was masking of the gasket lines and the use of robust-resistant weighting during data merging [50]. Data collections were taken at 0.18, 1.00, and 2.00 GPa for **1**·3CH_3CN and at 0.45, 1.23, 1.75, 3.00, and 4.55 GPa for **2**·2CH_3CN·1H_2O. Refinements of the compressed form of **1**·3CH_3CN and **2**·2CH_3CN·1H_2O were carried out starting from the coordinates obtained from a separate data collection carried out under ambient pressure and T = 150 K using MoK_α radiation on a Bruker Smart diffractometer [51]. The anomalous scattering factors and mass absorption coefficients were calculated with WINGX [52]. The program CRYSTALS [53] was used to refine the structures against F using all reflections with $I > 2\sigma(I)$.

In the ambient-pressure refinement of **1**·3CH_3CN the perchlorate anion based on Cl58/Cl63 is disordered in the ratio 60 : 40 over two orientations that share a common plane of three O atoms. The third anion, based on Cl55 was modelled with one ordered Cl–O axis, whilst the remaining three oxygen atoms disordered over three different orientations in the 45 : 35 : 20 ratio were restrained to be tetrahedral.

Due to the low completeness of the high-pressure data sets, the aromatic rings in **1**·3CH_3CN were treated as rigid bodies. All the perchlorate anions in **1**·3CH_3CN were ordered at high pressure, but tetrahedral restraints were applied. With the exception of Cl and Mn, all atoms were refined isotropically.

In **2**·2CH_3CN·1H_2O all non-H atoms were modelled with anisotropic displacement parameters. Similarity restraints were applied to chemically equivalent bond lengths and angles of the bpy ligands and PF_6 anions. At ambient pressure it was possible to model one molecule of CH_3CH explicitly with the remaining solvent being treated with the SQUEEZE routine [40]. All the solvent was modeled using SQUEEZE in the high-pressure refinements.

Refinement parameters are reported in Tables 1 and 2. Void diagrams were calculated [42] and visualised with MERCURY [54, 55]. The structures and packing diagrams were drawn using DIAMOND [55].

CCDC 763230 – 763239 contain the supplementary crystallographic data for this paper. These data can be obtained free of charge from The Cambridge Crystallographic Data Centre *via* www.ccdc.cam.ac.uk/data_request/cif.

Magnetic measurements

Variable-temperature dc magnetic susceptibility measurements were made on a Quantum Design Magnetic Property Measurement System (SQUID magnetometer) equipped with a 7 T magnet operating in the 350 – 2 K temperature range. Diamagnetic corrections were applied using Pascal's constants. For the high-pressure magnetic measurements a cell of piston-cylinder design was used [17]. The body of the pressure cell was made of CuBe alloy. A pellet of sample was put in the cell using Daphne 7373 oil (IDEMITSU-ILS) as the pressure-transmitting medium. Data were collected at 0.32, 0.54, and 0.87 GPa for **1**·3CH_3CN and at 0.36, 0.58, 0.84 GPa for **2**·2CH_3CN·1H_2O. The program MAGPACK [56] was used to simulate the susceptibility.

Acknowledgements

We wish to thank EPSRC (UK) for funding, the STFC for allocation of synchrotron beam time and Dr. Stephen Moggach and Mr. Russell Johnstone for their help with data collection during synchrotron beam time.

[1] B. Bleaney, K. D. Bowers, *Proc. Roy. Soc. London* **1952**, *A214*, 451.
[2] V. H. Crawford, H. W. Richardson, J. R. Wasson, D. J. Hodgson, W. E. Hatfield, *Inorg. Chem.* **1976**, *15*, 2107.
[3] W. E. Hatfield, *Comm. Inorg. Chem.* **1981**, *1*, 105.
[4] T. Cauchy, E. Ruiz, S. Alvarez, *J. Am. Chem. Soc.* **2006**, *128*, 15722.
[5] G. V. R. Chandramouli, T. K. Kundu, P. T. Manoharan, *Aust. J. Chem.* **2003**, *56*, 1239 – 1248.
[6] D. Gatteschi, O. Kahn, R. D. Willet, *Magneto Structural Correlation in Exchange Coupled Systems*, D. Reidel, Dordrecht, **1985**.
[7] J. Glerup, D. J. Hodgson, E. Petersen, *Acta Chem. Scand.* **1983**, *A37*, 161 – 164.
[8] F. Neese, *J. Am. Chem. Soc.* **2006**, *128*, 10213 – 10222.
[9] E. Ruiz, S. Alvarez, P. Alemany, *Chem. Comm.* **1998**, 2767 – 2768.
[10] H. Weihe, H. -U. Güdel, *J. Am. Chem. Soc.* **1998**, *120*, 2870 – 2879.
[11] R. Miletich, D. R. Allan, W. F. Kuhs, *Rev. Mineral. Geochem.* **2000**, *41*, 445 – 519.
[12] APEX-II (version V1), Area-Detector Integration Software, Bruker Analytical X-ray Instruments Inc., Madison, Wisconsin (USA), **2004**.
[13] A. Dawson, D. R. Allan, S. Parsons, M. Ruf, *J. Appl. Crystallogr.* **2004**, *37*, 410 – 416.
[14] S. Parsons, SHADE, The University of Edinburgh, Edinburgh (United Kingdom) **2004**.
[15] W. A. Bassett, *High Pressure Research* **2009**, *29*, 163.
[16] S. A. Moggach, D. R. Allan, S. Parsons, J. E. Warren, *J. Appl. Crystallogr.* **2008**, *41*, 249 – 251.
[17] K. V. Kamenev, S. Tancharakorn, N. Robertson, A. Harrison, *Rev. Sci. Instrum.* **2006**, *77*, 073905.
[18] J. Sanchez-Benitez, S. Tancharakorn, M. K. Hutchinson, K. V. Kamenev, *J. Phys.: Conf. Ser.* **2008**, *121*, 122001.
[19] D. R. Allan, S. Parsons, S. J. Teat, *J. Synchr. Rad.* **2001**, *8*, 10 – 17.
[20] D. R. Allan, S. J. Clark, *Phys. Rev. B* **1999**, *60*, 6328 – 6334.
[21] D. R. Allan, S. J. Clark, M. J. P. Brugmans, G. J. Ackland, W. L. Vos, *Phys. Rev. B* **1998**, *58*, R11809–R11812.
[22] D. R. Allan, S. J. Clark, S. Parsons, M. Ruf, *J. Phys.: Condens. Matt.* **2000**, *12*, L613–L620.
[23] E. V. Boldyreva, *J. Mol. Struct.* **2003**, *647*, 159 – 179.
[24] S. A. Moggach, S. Parsons, P. A. Wood, *Crystallogr. Rev.* **2008**, *14*, 143 – 184.
[25] I. D. H. Oswald, D. R. Allan, G. M. Day, W. D. S. Motherwell, S. Parsons, *Cryst. Growth Des.* **2005**, *5*, 1055 – 1071.
[26] S. A. Moggach, S. Parsons, *Spectroscop. Prop. Inorg. Organomet. Compd.* **2009**, *40*, 324 – 354.
[27] J. A. Hriljac, *Crystallogr. Rev.* **2006**, *12*, 181 – 193.
[28] G. G. Levchenko, E. E. Zubov, V. N. Varyukhin, A. B. Gaspar, J. A. Real, *J. Phys. Chem. B* **2004**, *108*, 16664 – 16669.
[29] M. Mito, H. Deguchi, T. Tajiri, S. Takagi, M. Yamashita, H. Miyasaka, *Phys. Rev. B* **2005**, *72*, 144421.
[30] A. Sieber, R. Bircher, O. Waldmann, G. Carver, G. Chauboussant, H. Mutka, H. -U. Güdel, *Angew. Chem.* **2005**, *117*, 4311 – 4314; *Angew. Chem. Int. Ed.* **2005**, *44*, 4239 – 4242.
[31] Y. Suzuki, K. Takeda, K. Awaga, *Phys. Rev. B* **2003**, *67*, 132402/1 – 132402/4.
[32] T. Tanaka, W. Fujita, K. Awaga, *Chem. Phys. Lett.* **2004**, *393*, 150 – 152.
[33] A. Prescimone, C. J. Milios, S. A. Moggach, J. E. Warren, A. R. Lennie, J. Sanchez-Benitez, K. Kamenev, R. Bircher, M. Murrie, S. Parsons, E. K. Brechin, *Angew. Chem.* **2008**, *120*, 2870 – 2873; *Angew. Chem. Int. Ed.* **2008**, *47*, 2828 – 2831.
[34] A. Prescimone, C. J. Milios, J. Sanchez-Benitez, K. Kamenev, C. Loose, J. Kortus, S. A. Moggach, M. Murrie, J. E. Warren, A. R. Lennie, S. Parsons, E. K. Brechin, *Dalton Trans.* **2009**, 4858 – 4867.
[35] A. Prescimone, S. A. Moggach, J. Sanchez-Benitez, K. V. Kamenev, J. E. Warren, A. R. Lennie, S. Parsons, E. K. Brechin, *Inorg. Chem.* **2009**, submitted.
[36] A. Prescimone, J. Sanchez-Benitez, K. Kamenev, S. A. Moggach, M. Murrie, J. E. Warren, A. R. Lennie, S. Parsons, E. K. Brechin, *Dalton Trans.* **2009**, 7390 – 7395.
[37] A. Prescimone, J. Sanchez-Benitez, K. Kamenev, S. A. Moggach, J. E. Warren, A. R. Lennie, S. Parsons, E. K. Brechin, *Dalton Trans.* **2010**, in print.
[38] A. Bencini, D. Gatteschi, *EPR of Exchange Coupled Systems*, Springer Verlag, Berlin, **1990**.
[39] P. M. Plaksin, R. C. Stoufer, M. Mathew, G. J. Palenik, *J. Am. Chem. Soc.* **1972**, *94*, 2121 – 2122.
[40] P. Van der Sluis, A. L. Spek, *Acta Crystallogr.* **1990**, *A46*, 194 – 201.

[41] S. A. Moggach, T. D. Bennett, A. Cheetham, *Angew. Chem.* **2009**, *121*, 7221 – 7223; *Angew. Chem. Int. Ed.* **2009**, *48*, 7087 – 7089.

[42] A. L. Spek, PLATON, A multipurpose Crystallographic Tool, Utrecht University, Utrecht (The Netherlands), **2004**. See also: A. L. Spek, *J. Appl. Crystallogr.* **2003**, *36*, 7 – 13.

[43] R. I. Cooper, G. C. Dismukes, M. P. Klein, M. Calvin, *J. Am. Chem. Soc.* **1978**, *100*, 7248 – 7252.

[44] M. Stebler, A. Ludi, H. -B. Bürgi, *Inorg. Chem.* **1986**, *25*, 4743 – 4750.

[45] S. R. Cooper, M. Calvin, *J. Am. Chem. Soc.* **1977**, *99*, 6623 – 6630.

[46] L. Merrill, W. A. Bassett, *Rev. Sci. Instrum.* **1974**, *45*, 290 – 294.

[47] G. J. Piermarini, S. Block, J. D. Barnett, R. A. Forman, *J. Appl. Phys.* **1975**, *46*, 2774 – 2780.

[48] SAINT (version 7), Bruker Analytical X-ray Instruments Inc., Madison, Wisconsin (USA) **2006**.

[49] G. M. Sheldrick, SADABS (version 2004-1), Program for Empirical Absorption Correction of Area Detector Data, University of Göttingen, Göttingen (Germany) **2004**.

[50] R. H. Blessing, *J. Appl. Crystallogr.* **1997**, *30*, 421 – 426.

[51] SMART, Area-Detector Software Package, Bruker Analytical X-ray Instruments Inc., Madison, Wisconsin (USA) **2002**.

[52] L. J. Farrugia, WINGX, A MS-Windows System of Programs for Solving, Refining and Analysing Single Crystal X-ray Diffraction Data for Small Molecules, University of Glasgow, Glasgow, Scotland (United Kingdom) **2005**. See also: L. J. Farrugia, *J. Appl. Crystallogr.* **1999**, *32*, 837 – 838.

[53] D. J. Watkin, K. Prout, J. R. Carruthers, P. W. Betteridge, R. I. Cooper, CRYSTALS (issue 12), Chemical Crystallography Laboratory, University of Oxford, Oxford (United Kingdom) **2003**.

[54] C. F. Macrae, I. J. Bruno, J. A. Chisholm, P. R. Edgington, P. McCabe, E. Pidcock, L. Rodriguez-Monge, R. Taylor, J. Van de Streek, P. A. Wood, *J. Appl. Cryst.* **2008**, *41*, 466 – 470.

[55] K. K. Brandenburg, DIAMOND, Crystal and Molecular Structure Visualization, Crystal Impact – K. Brandenburg & H. Putz GbR, Bonn (Germany) **2005**.

[56] J. J. Borrás-Almenar, J. M. Clemente-Juan, E. Coronado, B. S. Tsukerblat, *J. Comput. Chem.* **2001**, *22*, 985 – 991.